The Effect of Aluminum in Shielded Metal Arc C-Mn Steel Multipass Deposits

Hardness and toughness are most affected by varying levels of aluminum in the weld metal

BY G. M. EVANS

ABSTRACT. The effect of varying the aluminum content of an E7018-type electrode on weld metal composition, microstructure and properties has been studied. This investigation found that aluminum modified the as-deposited and reheated microstructure and changed the composition of the nonmetallic inclusions. The weld metal hardness and tensile properties increased with increasing aluminum, and optimum impact properties, for both the as-welded and the stress-relieved condition, were exhibited at zero aluminum and somewhat less favorably at an intermediate aluminum content of approximately 350 ppm.

Introduction

This investigation forms part of a joint program, within Subcommission II A of the International Institute of Welding, to study the factors affecting the microstructure and properties of multipass shielded metal arc welds. Previous work has examined the process parameters (Ref. 1) and considered the relative effects of the main elements occurring in mild steel weld metal, namely carbon (Refs. 2, 3), manganese (Refs. 1-3), silicon (Ref. 4), sulfur (Ref. 5) and phosphorus (Ref. 5). The influence of weld metal aluminum content has now been evaluated as one of the initial steps in the process of understanding the role of residual elements in multipass weldments.

Aluminum is introduced into SMA welds either by dilution from the base plate or from the coating and the core wire. Continuous cast wires, in particular, are a possible source of aluminum and, since the cost advantage and availability of "rimmed" steel produced by the ingot route are being progressively eroded, it is of practical importance to quantify the effect of the element.

G. M. EVANS is with Welding Industries Oerlikon Buhrle Ltd., Zurich, Switzerland.

Paper presented at the 71st Annual AWS Meeting, held April 22-27, 1990, in Anaheim, Calif.

Experimental Procedure

Electrodes

A balanced range of nine experimental basic iron powder-type electrodes was prepared by progressively increasing the amount of aluminum powder in the coating, up to a maximum of 7%. The consumables were of the C type, according to a previous designation (Refs. 1-4), and yielded weld metals with a nominal composition of 0.08% C, 1.4% Mn and 0.35% Si. The rimmed core wire employed was 4-mm (0.16-in.) diameter and the coating factor (D/d) was 1.68.

Weld Preparation

The joint geometry was that specified in ISO 2560, 1973. Welding was done in the flat position and three beads per layer were deposited (Ref. 1). The total number of runs required to fill the individual joints was 27. Direct current (electrode positive) was employed, the amperage being 170 A, the arc voltage 21 V and the nominal heat-input 1 kJ/mm (25 kJ/in.). The interpass temperature was standardized at 200°C (392°F).

KEY WORDS

Effect of Aluminum
E7018 Electrode
Aluminum in E7018
Inclusion Composition
Nonmetallic Inclusions
Al Effect on Impact
Multipass SMA Welds
Residual Elements
Microstructure Effects
IIW Subcommission IIA

Mechanical Testing

Two subsize all-weld-metal tensile specimens were machined and tested for each of the different deposits. Also, approximately 35 Charpy V-notch specimens were struck, so as to obtain a full transition curve. The impact specimens were in the as-welded condition, whereas the tensile specimens were given a hydrogen removal treatment at 250°C (484°F) for 14 hours.

Metallography

Transverse sections were prepared, and detailed examination was carried out on the top beads and on the adjacent supercritically reheated zones, as described previously (Refs. 1-4). Nonmetallic inclusions in six of the weldments were chemically analyzed using an SEM-based automatic image analyzer, and the mean three-dimensional particle diameter was determined (Ref. 6).

Results

Chemical Composition

The chemical analyses of the nine all-weld-metal deposits studied are given in Table 1. Carbon was essentially constant, but manganese and silicon tended to be unbalanced for the last three weldments of the series. As expected, increasing amounts of aluminum were transferred into the deposits, as shown in Fig. 1. Titanium was successfully balanced and, rather fortunately, oxygen remained invariable. On the other hand, residual and total nitrogen contents decreased with increasing aluminum, as depicted in Fig. 2.

Metallographic Examination

General—Macro examination of the weldments revealed no essential differences with regard to segregation or the degree of recrystallization, which was approximately 70-80% at the Charpy V-

Table 1—Chemical Composition of Weld Deposits[a]

Code	Aluminum in coating, %	C	Mn	Si	S	P	Al[b]	Ti[b]	O[c]	N[d] Total	N[e] Residual
				%					ppm		
P	0	0.069	1.36	0.30	0.007	0.009	<5	37	432	67	33
–	1	0.073	1.39	0.33	0.007	0.008	20	39	427	66	n.d.
–	2	0.078	1.39	0.32	0.007	0.009	44	42	436	66	n.d.
Q	3	0.080	1.41	0.33	0.006	0.009	78	43	432	61	34
–	4	0.080	1.42	0.37	0.006	0.009	120	43	439	54	n.d.
–	5	0.076	1.36	0.37	0.005	0.009	190	36	422	54	24
R	6	0.078	1.31	0.44	0.005	0.008	340	36	431	52	18
–	6.5	0.076	1.30	0.51	0.005	0.008	490	43	423	50	17
S	7	0.079	1.32	0.57	0.004	0.008	610	38	422	48	18

(a) Nb, V, B: <5 ppm.
(b) ICP-AES.
(c) BALZERS.
(d) LECO;.
(e) TWI, ref. 7.

notch location (Ref. 1). However, the average columnar grain width in the top beads was observed to differ, firstly increasing with increasing aluminum, then decreasing and finally increasing again, as indicated in Fig. 3.

As-Deposited Weld Metal—Top beads of six chosen deposits were optically examined and metallographic measurements were made, following the current guidelines (Ref. 8) of IIW Subcommission IX J, to quantify the major microstructural components, namely: primary ferrite (PF), ferrite with second phase (FS) and acicular ferrite (AF).

The point count results obtained are plotted in Fig. 4 and reveal a complex situation. Initially, aluminum induced a decrease in the volume fraction of acicular ferrite before increasing the amount and then subsequently decreasing it again. The changes were compensated for by a reverse trend in the volume fraction of ferrite with second phase, the amount of primary ferrite remaining relatively constant.

Photomicrographs of as-deposited columnar regions of welds containing 5, 78, 340 and 610 ppm Al—designated P, Q, R and S, respectively—are shown at ×100 magnification in Fig. 5. Of note, even at this low magnification, is the coarse structure exhibited at the highest level of aluminum investigated. Further detail, illustrating columnar regions, is shown in Fig. 6. Ferrite with second phase is particularly evident in S, and coarsening of the acicular ferrite laths and the associated microphases is seen to have occurred.

Reheated Weld Metal—Examination of the high-temperature regions directly below the top beads revealed similar changes to those encountered in the as-deposited metal, as shown in Fig. 7. In the extreme case (S), ferrite envelopes still delineated the prior austenite grain boundaries, but ferrite with aligned second phase had replaced approximately 50% of the fine acicular structure within the grains.

Modifications were also observed in the low-temperature reheated regions, as seen in Fig. 8, on comparison of the two extreme aluminum levels, P and S. Grain size measurements (Ref. 9) are plotted in Fig. 9 and indicate grain refinement up to approximately 300 ppm Al and thereafter a slight grain coarsening. At high aluminum contents, however, the so-called fine-grained reheated regions became more duplex in character, and increasing difficulty in measurement, at the recommended (Ref. 9) magnification of 630X, was encountered. The same problem has been reported on adding major alloying elements, such as Mo (Ref. 10) and Cr (Ref. 11), to the C-Mn system.

More detailed examination, using the scanning electron microscope (SEM), revealed that the microphases associated with the equiaxed ferrite grains were martensite/austenite (M/A) and cementite films. Little change in microphase morphology could be detected with increasing aluminum, and the volume fraction increased only marginally from 8 up to approximately 10%. The grain boundary cementite films, however, were perceptibly thicker and possibly more continuous at high aluminum contents, as seen on comparison of the two micrographs shown in Fig. 10.

Nonmetalic Inclusions

Six deposits were examined (Ref. 6) at SINTEF (Norway) to determine the composition of the inclusions and the mean

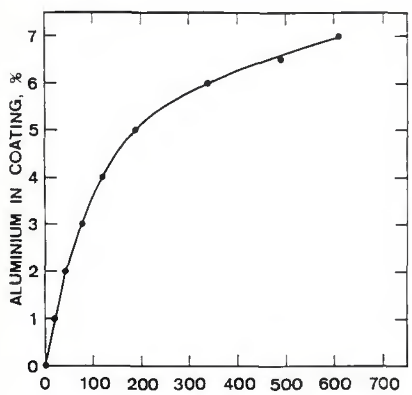

Fig. 1—Plot of aluminum in electrode coating against aluminum in weld metal.

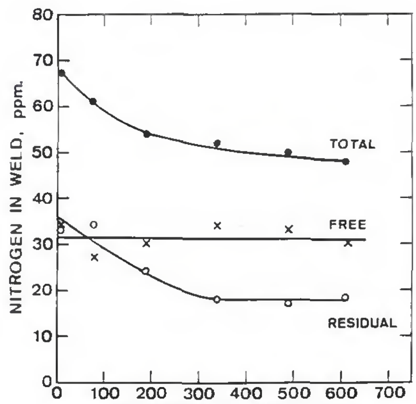

Fig. 2—Plot of residual, free and total nitrogen content against aluminum in weld metal.

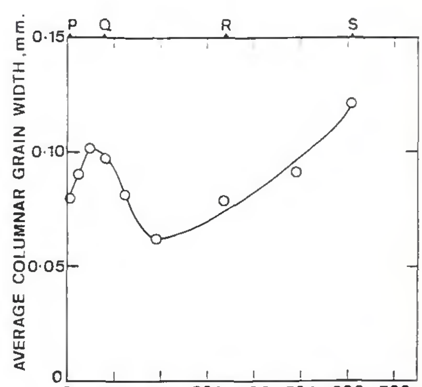

Fig. 3—Effect of aluminum on the average columnar grain width (top bead).

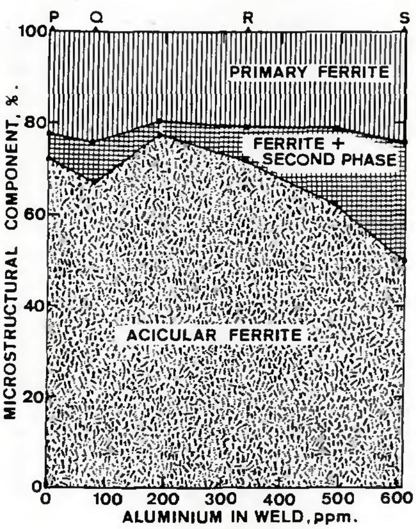

Fig. 4—Effect of aluminum on the microstructure of as-deposited weld metal.

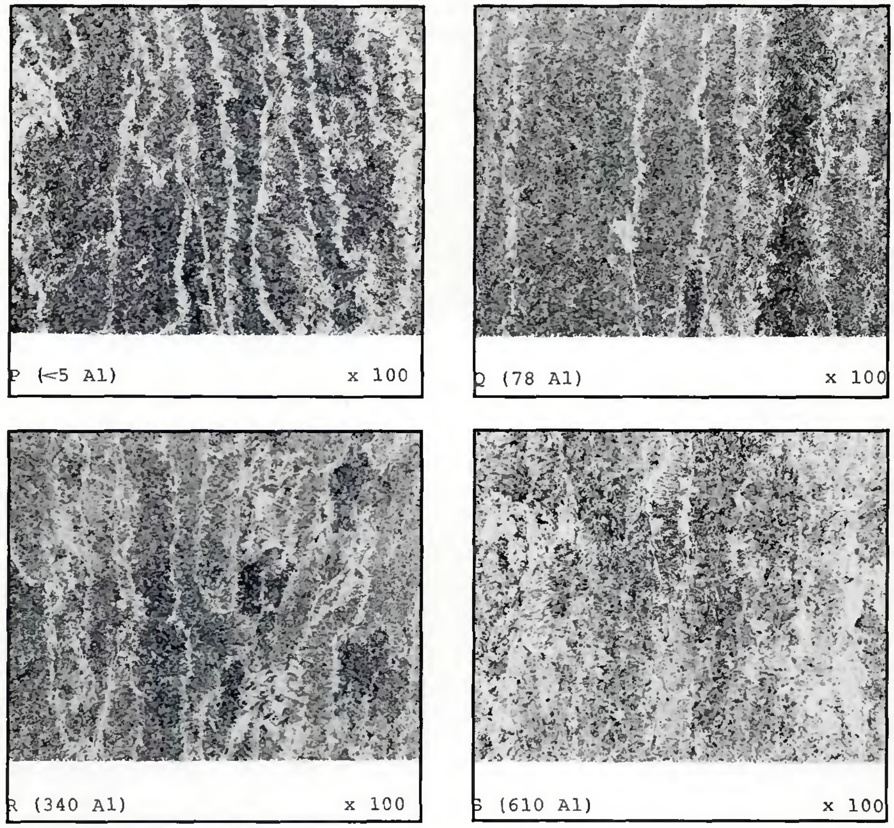

Fig. 5—Photomicrographs of top beads (different aluminum contents).

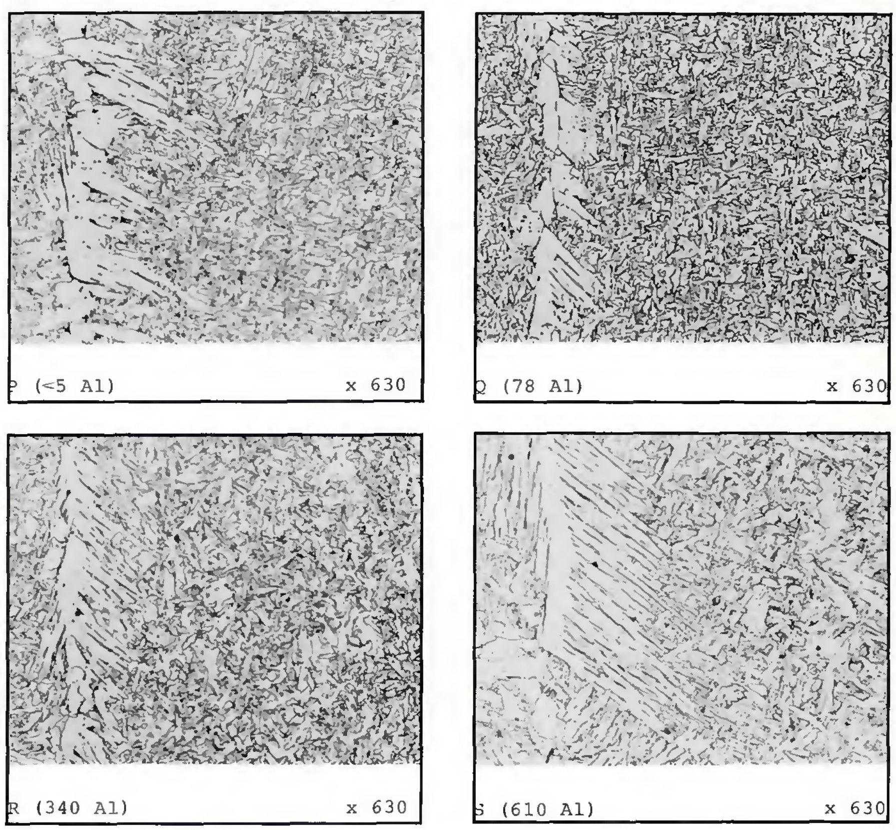

Fig. 6—Photomicrographs of top beads (different aluminum contents).

three-dimensional particle diameter. The analytical results are plotted in Fig. 11 and show that MnO and SiO_2 were progressively replaced by Al_2O_3. The data are superimposed on the tertiary Al_2O_3-MnO-SiO_2 diagram in Fig. 12. The Si to Mn ratio in the deoxidation products was relatively constant and significantly higher than that of stoichiometric Rhodonite (MnO · SiO_2). At the zero aluminum level, some pure silica inclusions were identified, but otherwise most particles contained measurable amounts of both sulfur and copper.

Histograms of inclusion size distributions, based in each case on measurement of 500 particles, are presented in Fig. 13. The arithmetic mean three-dimensional diameter was virtually independent of the weld metal aluminum content, varying at the most between 0.32 and 0.38 μm. Also, it was ascertained that the average aspect ratio of the particles, determined as being approximately 1.2, was essentially independent of the aluminum level.

Examination of replicated inclusions in the scanning transmission electron microscope (STEM) revealed that high-aluminum-containing inclusions were rarely acting as nucleation sites for acicular ferrite formation in as-deposited weld metal. Examples for the two extremes are shown in Fig. 14. At low aluminum, the inclusion is typically a nucleating MnO · SiO_2 particle associated with surface compounds containing Mn, Cu, S and sporadically a high local concentration of Ti. The high aluminum example in Fig. 14 is an inert Al_2O_3 inclusion. Manganese, copper and sulfur were found near the surface, but little trace of titanium could be detected. Of note, at high aluminum contents, was a tendency for the inclusions to cluster and even impinge in some cases.

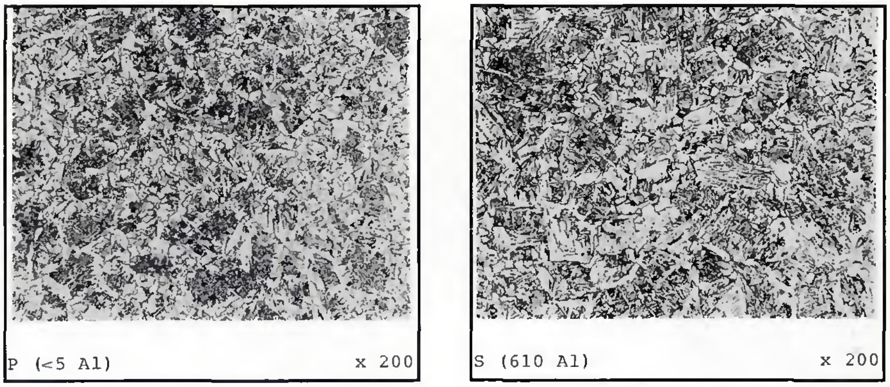

Fig. 7 — Photomicrographs of the high-temperature reheated regions (low- and high-aluminum contents).

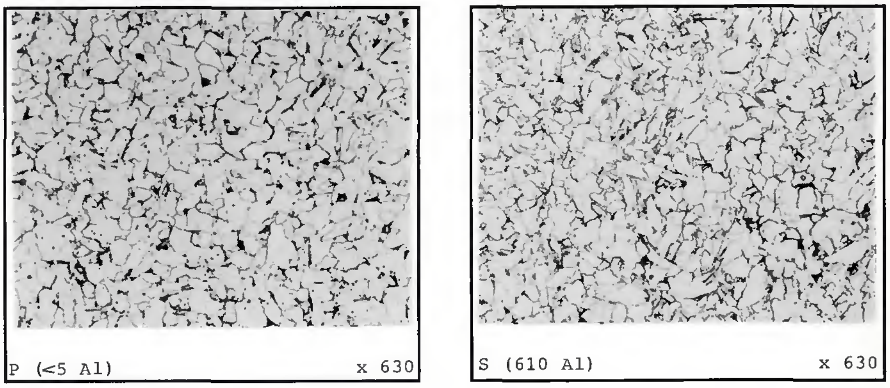

Fig. 8 — Photomicrographs of the low-temperature reheated regions (low- and high-aluminum contents).

Mechanical Properties

Hardness Testing — Average hardness values obtained for the top beads are plotted in Fig. 15. Apart from a slight initial and final drop, a generally increasing trend in hardness is depicted with increasing aluminum.

Tensile Results — The tensile test data are presented in Table 2. The yield and tensile strengths are plotted against weld metal aluminum content in Fig. 16 and show a generally increasing but nonlinear trend. The change, however, is slight and possibly influenced by the imbalance in silicon (Ref. 4).

Impact Results — Charpy V-transition curves obtained for six of the nine weldments are drawn in Figs. 17 and 18 for the as-welded and the stress-relieved condi-

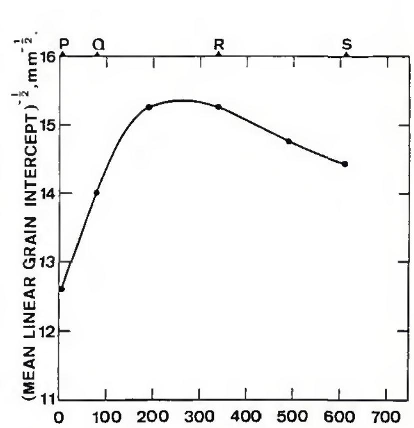

Fig. 9 — Effect of aluminum on the grain intercept in the low-temperature reheated region.

Table 2—Mechanical Test Results

Aluminum in Weld, ppm	As-Welded σ_E N/mm^2	As-Welded σ_R N/mm^2	As-Welded El %	As-Welded RA %	Stress-Relieved (2 h/580°C) σ_E N/mm^2	Stress-Relieved σ_R N/mm^2	Stress-Relieved El %	Stress-Relieved RA %
<5	468	529	32.6	80.7	393	500	31.8	77.0
20	475	536	33.4	80.7	387	493	32.5	80.7
44	478	541	30.4	78.9	398	499	32.8	80.7
78	478	540	31.2	80.7	391	504	31.8	78.9
120	480	543	29.0	78.9	397	518	31.0	79.8
190	485	549	31.4	79.8	403	519	29.1	78.9
340	491	564	28.2	78.9	409	528	31.0	78.9
490	485	560	25.2	78.9	417	528	29.0	78.9
610	491	570	29.2	77.0	443	550	29.4	76.0

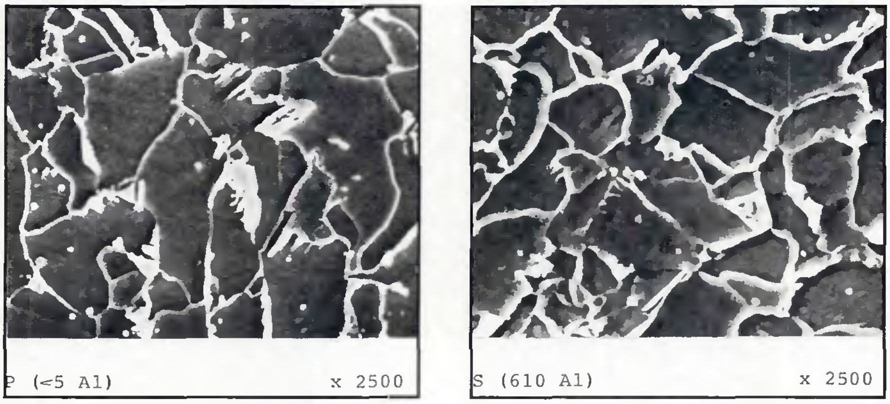

Fig. 10 — Microphases in the low-temperature reheated regions (low- and high-aluminum contents).

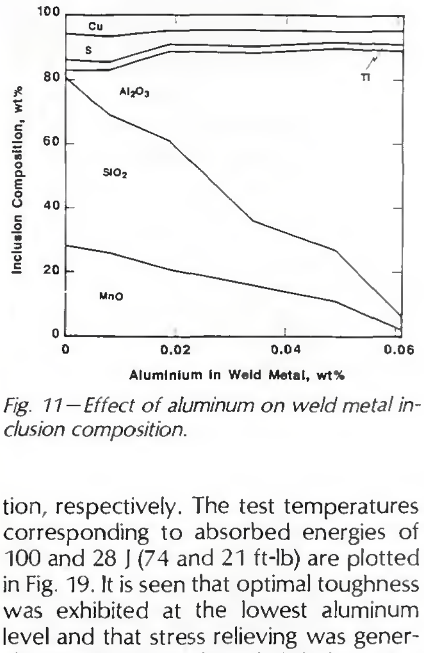

Fig. 11 — Effect of aluminum on weld metal inclusion composition.

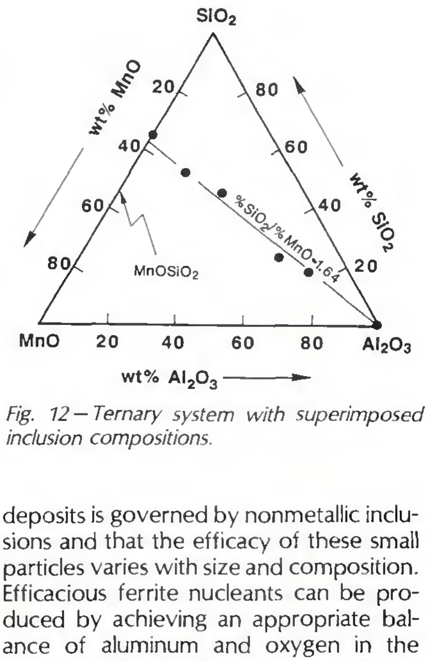

Fig. 12 — Ternary system with superimposed inclusion compositions.

tion, respectively. The test temperatures corresponding to absorbed energies of 100 and 28 J (74 and 21 ft-lb) are plotted in Fig. 19. It is seen that optimal toughness was exhibited at the lowest aluminum level and that stress relieving was generally beneficial; the lateral shift for 100 J ranging between −8° and −15°C.

The temperatures corresponding to 100 J are reconsidered in Fig. 20 against the Al:O ratio. Three distinct domains are evident, increasing aluminum being first deleterious, then beneficial, as the ratio increased from 0.2 to approximately 0.8, and finally deleterious again as the value exceeded 0.8.

Discussion

In reviewing the relevant literature, which deals almost exclusively with submerged arc welding, Abson (Ref. 12) concluded that the microstructure of weld deposits is governed by nonmetallic inclusions and that the efficacy of these small particles varies with size and composition. Efficacious ferrite nucleants can be produced by achieving an appropriate balance of aluminum and oxygen in the welds, and thus in the inclusions, or by introducing a sufficient level of Ti. An excess of aluminum was considered detrimental, even in the presence of a significant level of Ti, and it was postulated that a dearth of Al is not deleterious when sufficient Ti is present. Harrison (Ref. 13) further reviewed the factors influencing the toughness of line pipe welds and concluded, from the work of Thewlis (Ref. 14), that an optimum Al:O ratio of 0.84 is desirable, *i.e.*, corresponding to the stoichiometry of galaxite ($Al_2O_3 \cdot MnO$). Similarly, from the data of Saggese, *et al.* (Ref. 15), and of Bonnet and Charpentier (Ref. 16), it was proposed that the Ti:O ratio be optimized at 0.1.

In order to study the role of aluminum in isolation, an attempt was made in the present investigation to balance the weld metal composition. This was achieved by progressively reducing the amount of manganese and ferro-silicon in the coating, as aluminum was added. The deoxidation potential was maintained and weld metal oxygen remained constant. The amount of titanium in the welds was additionally balanced, and by a judicious choice of raw material (Ref. 17), the background level of Nb, V and B was kept low (<5 ppm). The total nitrogen content, however, tended to decrease, due presumably to dilution by aluminum vapor in the arc atmosphere. The residual nitrogen also decreased, whereas, the free nitrogen remained essentially unchanged. Thus, in accord with the work of Terashima and Hart (Ref. 18), it can be concluded that aluminum nitride formation does not occur at the cooling rates involved.

Metallographic examination of top beads revealed that aluminum induced a change in the average columnar grain width, initial coarsening being followed by refinement and subsequently by coarsening again above 200 ppm. According to Kluken, *et al.* (Ref. 19), nonmetallic inclusions play a critical role in the development of the columnar grain structure by acting as inert substrates for nucleation of delta ferrite ahead of the advancing interface. The modifications to the prior austenite grain size were accompanied by equivalent changes in the volume fraction of ferrite with second phase, a minimum being attained at 200 ppm Al. Complex austenite grain size/transformation temperature characteristics have recently been reported by Thewlis (Ref. 20) as due largely to changes in inclusion composition. It was proposed that TiO/TiN and galaxite are particularly active substrates for increasing the propensity to intragranular ferrite formation. Several interrelated effects are operative, and at this stage, it can only be surmised that the TiO/TiN present on the surface layers of manganese silicate particles was progressively modified. Initially, acicular ferrite decreased as aluminum was added and the formation of complex spinels is assumed, as encountered on adding sulfur (Ref. 5). At the stage at which the prior austenite grain size decreased, it is concluded that galaxite became an active component. Finally, with increasing Al_2O_3, transformation was modified, and increasing difficulty was encountered in promoting acicular ferrite. Of interest is the fact that the change in average composition of the inclusions was not accompanied by a difference in size distribution.

The hardness of the top beads generally increased with increasing aluminum, apart from a slight initial and final drop. The former could possibly be associated with

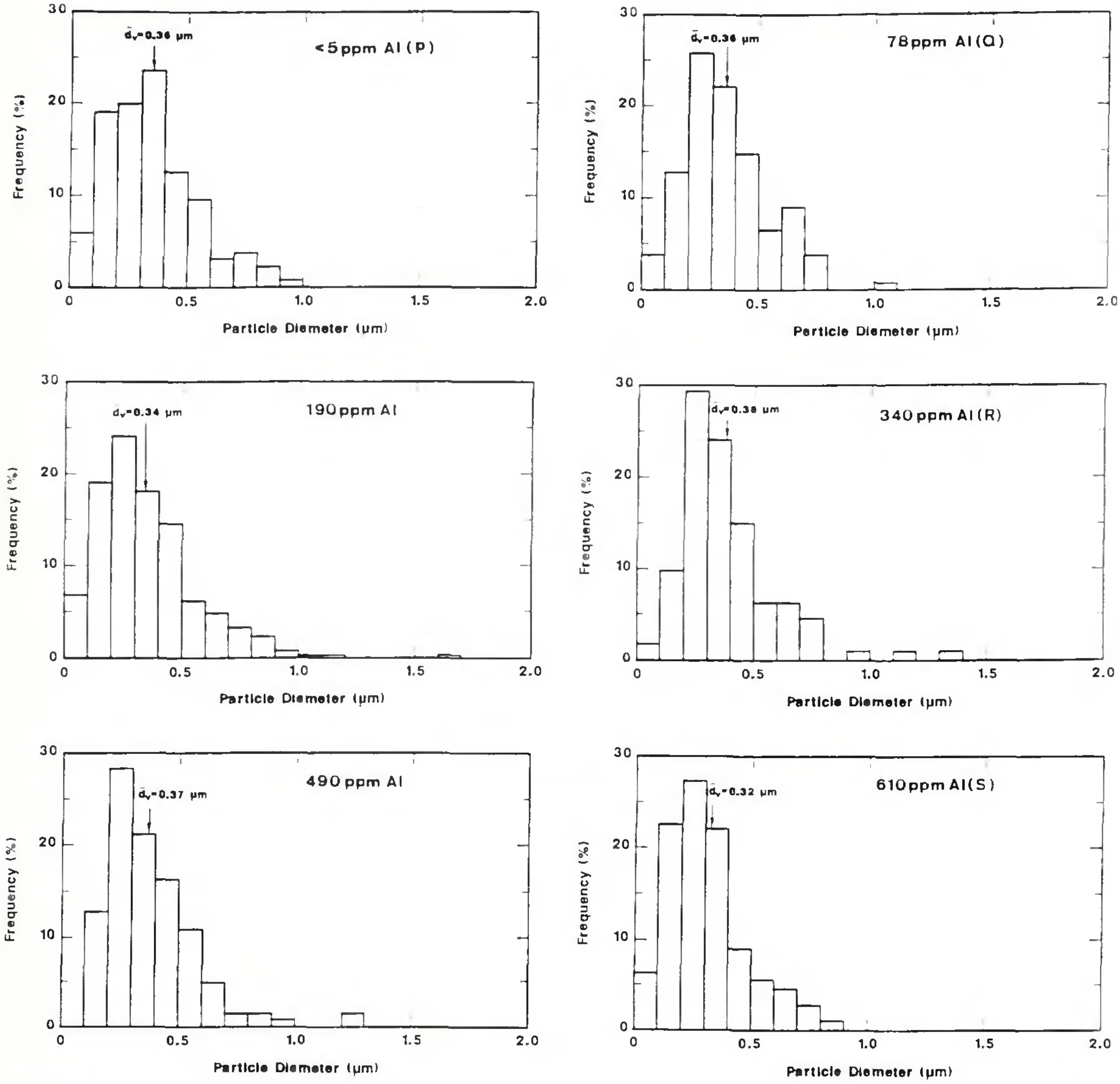

Fig. 13 — Particle size distribution of nonmetallic inclusions.

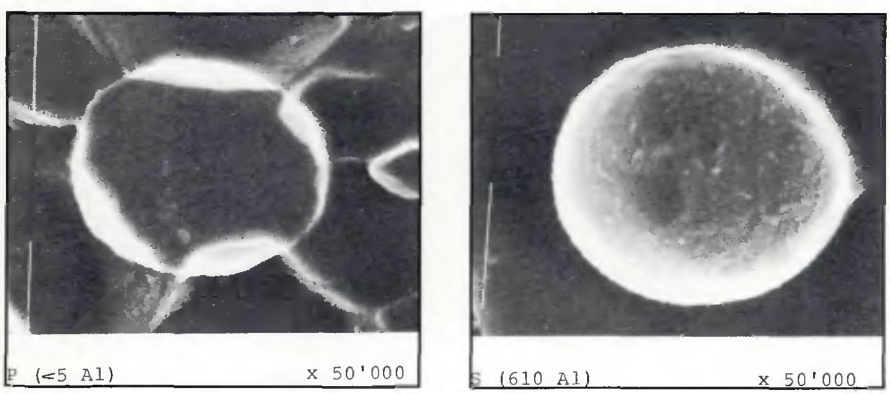

Fig. 14 — STEM micrographs of replicated inclusions in low- and high-aluminum-containing welds.

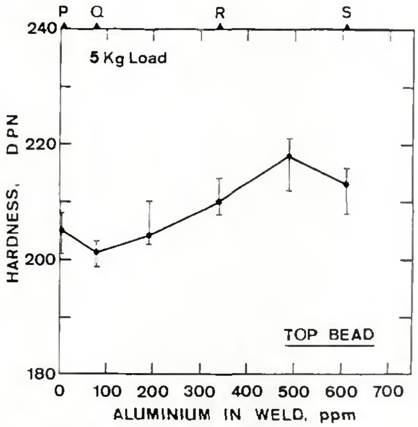

Fig. 15 — Hardness of top bead plotted against weld metal aluminum content.

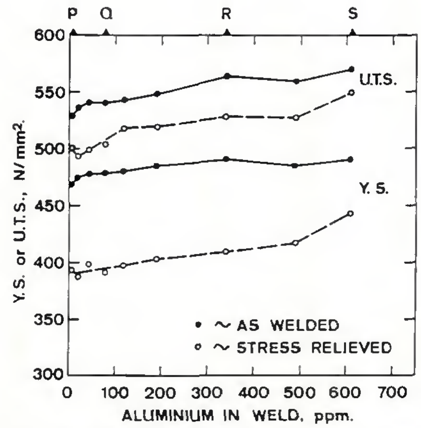

Fig. 16 — Yield and ultimate tensile strengths plotted against weld metal aluminum content.

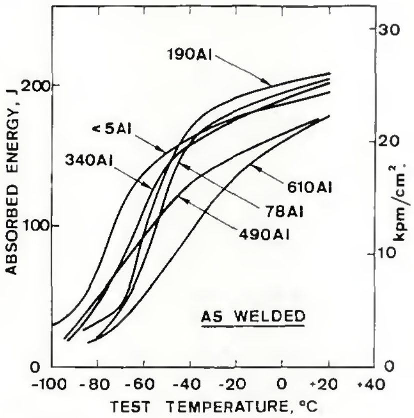

Fig. 17 — Charpy V-notch transition curves (as-welded condition).

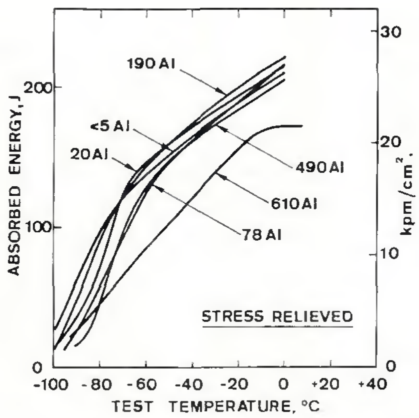

Fig. 18 — Charpy V-notch transition curves (stress-relieved condition).

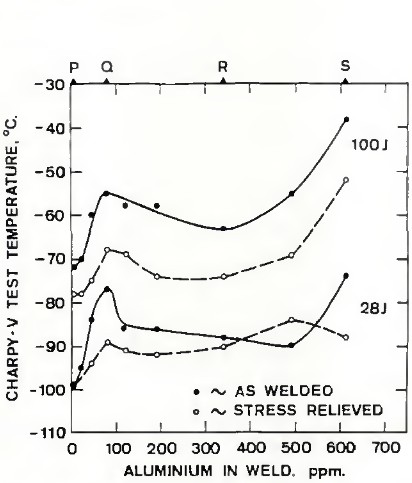

Fig. 19 — Effect of aluminum on the Charpy V-notch test temperature corresponding to 100 and 28 J.

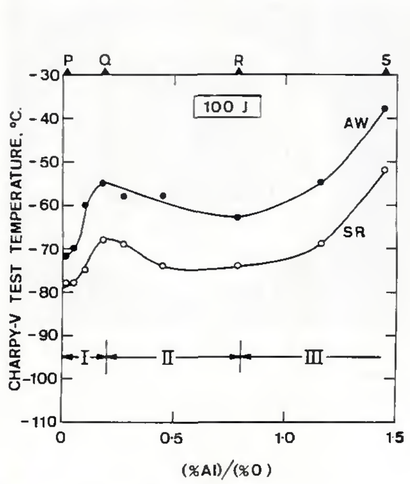

Fig. 20 — Charpy V-notch test temperature corresponding to 100 J plotted against Al:O ratio.

a microstructural change but no explanation other than scattering can be put forward for the location of the latter. The bulk tensile properties generally increased monotonically with aluminum content, with little evidence of microstructural dependence. The change was slight and overshadowed to a certain extent by variations in C, Mn and Si. Postweld heat treatment resulted in a reduction of the tensile parameters, especially the yield stress. The change was substantially greater than that encountered previously (Ref. 3), due to the absence of Nb and V in the present instance.

The lowest impact transition temperature was obtained for the aluminum free deposit. On increasing aluminum, the notch toughness depreciated rapidly but then improved above 80 ppm Al. Subsequently, a second reversal occurred, and the situation deteriorated again above an aluminum content of about 350 ppm.

Three domains are thus indicated, the first coinciding well with the microstructural change encountered in the as-deposited metal. The final reversal, however, corresponding to an Al:O ratio of 0.8, was displaced to a higher concentration than that encountered for the maximum degree of acicularity. The Charpy V-notch was located in the bulk of the deposit, which had undergone recrystallization, and evidently other factors, not directly linked with acicular ferrite, were operative at high aluminum content. The reason is not understood but could be due either to differences in the amount of ferrite with aligned second phase in the high-temperature reheated regions or to grain boundary carbide morphology in the low-temperature reheated regions. Of note is the fact that the grain size measurements in the latter region failed to distinguish any difference between 200 and 350 ppm Al. Apart from one instance, postweld heat treatment improved notch toughness, and the same trend was exhibited as for the as-welded condition. The lateral shift induced by grain boundary carbide formation (Ref. 3) was substantial and enhanced by the absence of vanadium in the present case.

For the aluminum-free electrode, less than 5 ppm Al was found in the deposit. On the basis of the impact data, it is predicted that dilution with aluminum-containing base metal, in a root situation, for example, would have a deleterious effect. Similarly, the evidence suggests that the use of an aluminum-containing continuously cast core wire would also have a negative influence on notch toughness. The amount of aluminum introduced would probably not exceed 80 ppm and, in consequence, the situation could only be alleviated by additionally introducing aluminum via the coating. Unfortunately, Al powder detrimentally affects the running characteristics of the electrodes, and a compromise is required in practice.

The present study is limited to the extent that the results are specific to a weld metal oxygen content of 430 ppm and, consequently, other degrees of deoxidation are currently being explored, so as to define the Al-O system. In addition, since the titanium level in the present case was standardized, further work is envisaged to characterize the Al-Ti system. By this means, it is intended to separate the individual roles of aluminum and titanium and clarify the influence of nonmetallic inclusion interfaces on solidification substructure, prior austenite grain size and acicular ferrite formation. The basis for the work has already been set, the Mn-O system having been studied (Ref.17) in the absence of both aluminum and titanium.

Conclusions

For a balanced basic low-hydrogen electrode, of a specific slag base type, the following occurred on increasing from zero the amount of aluminum in the coating:

1) The microstructure of as-deposited weld metal was modified, with the volume fraction of acicular ferrite initially decreasing, then increasing and finally decreasing again.

2) The mean composition of the nonmetallic inclusions changed, MnO and SiO_2 being progressively replaced by Al_2O_3.

3) The hardness of as-deposited metal tended, in the main, to increase.

4) The tensile properties of the deposits marginally increased.

5) Optimum notch toughness characteristics were exhibited at the zero aluminum level.

6) Following degradation from zero aluminum, a small recovery in toughness was encountered at an aluminum content of 350 ppm.

Acknowledgments

The author is indebted to Mr. R. Züllig for assistance with the conventional metallographic part of the work. Thanks are also extended to Dr. M. Es-Souni, G.K.S.S., for conducting the electron microscopic studies, and to Dr. A. O. Kluken and Prof. Ø. Grong, SINTEF (Norway) for investigating the nonmetallic inclusions under contract.

References

1. Evans, G. M. 1983. Factors affecting the microstructure and properties of C-Mn all-weld-metal deposits. *Weld. Research Abroad,* WRC, 28 (1):1-69, also IIW Doc. II-983-82.

2. Evans, G. M. 1983. The effect of carbon on the microstructure and properties of C-Mn all-weld-metal deposits. *Welding Journal* 62 (11):313-s to 320-s.

3. Evans, G. M. 1986. The effect of stress-relieving on the microstructure and properties of C-Mn all-weld-metal deposits. *Welding Journal* 65 (12):326-s to 334-s.

4. Evans, G. M. 1986. The effect of silicon on the microstructure and properties of C-Mn all-weld-metal deposits. *Metal Construction* 18 (7):438R-444R.

5. Evans, G. M. 1986. The effect of sulfur and phosphorus on the microstructure and properties of C-Mn all-weld metal deposits. *Metal Construction* 18 (10):631R-646R.

6. Kluken, A. O., Grong, Ø., and Hjelen, J. 1988. SEM based automatic analysis of nonmetallic inclusions in steel weld metals. Mat. Sci. Techn., 4:649-654.

7. Stevens, S. M. 1989. Derivation of a procedure for determining free nitrogen in ferritic steels. Welding Institute Members Research Report, 406.

8. Guidelines for classification of ferritic steel weld metal microstructural constituents using the light microscope. 1986. *Weld. in the World,* (7/8)24:144-149;also IIW Doc. IX-1377-85.

9. Davey, T. G., and Widgery, D. J. 1976. A technique for the characterization of weld metal microstructures. IIW Doc. II-A-389-76.

10. Evans, G. M. 1988. The effect of molybdenum on the microstructure and properties of C-Mn all-weld-metal deposits. *Joining and Materials* 1(5):239-246.

11. Evans, G. M. 1989. The effect of chromium on the microstructure and properties of C-Mn all-weld-metal deposits. *Welding and Metal Fab.* 57(7): 346-358.

12. Abson, D. J. 1987. Small particles in weld metals — a review. IIW Doc. IX J-122-87.

13. Harrison, P. L. 1989. Factors influencing the toughness of submerged arc welded line pipe welds. The Welding Institute Bulletin, pp. 12-15 and 64-67.

14. Thewlis, G. 1986. The influence of pipe plate and consumable chemistry on the composition, microstructure and toughness of weld metal. *Proc. Conf. Welding and Performance of Pipelines.* The Welding Institute, London, England, pp. 205-227.

15. Saggese, M. E., Bhatti, A. R., Hawkins, D. N., and Whiteman, J. A. 1983. Factors influencing inclusion chemistry and microstructure in submerged arc welds. *Proc. Conf. The Effects of Residual, Impurity and Micro-Alloying Elements.* The Welding Institute, London, England, Paper 15.

16. Bonnet, C., and Charpentier, J.-P. 1983. Effect of deoxidation residues in wire and of some particular oxides in CS fused fluxes on the microstructure of submerged-arc weld metals. *Ibid,* Paper 8.

17. Abson, D. J., and Evans, G. M. 1989. A study of the manganese-oxygen system in low-hydrogen MMA all-weld-metal deposits. *Second International Conf. Trends in Welding Research,* Gatlinburg, Tenn.

18. Terashima, H., and Hart, P. H. M. 1983. Effect of flux TiO_2 and wire Ti content on tolerance to high Al content of submerged arc welds made with basic fluxes. *Proc. Conf. The Effects of Residual, Impurity and Microalloying Elements,* The Welding Institute, London, England, Paper 27.

19. Kluken, A. O., Grong, Ø., and Rørvik, G. Solidification microstructures and phase transformations in Al-Ti-Si-Mn deoxidized steel weld metals. Report N°. STF 34 A 89110, SINTEF, Trondheim, Norway.

20. Thewlis, G. Transformation kinetics of weld metal. British Steel technical report, to be published.

WRC Bulletin 343
May 1989

Destructive Examination of PVRC Weld Specimens 202, 203 and 251J

This Bulletin contains three reports:

(1) Destructive Examination of PVRC Specimen 202 Weld Flaws by JPVRC
By Y. Saiga

(2) Destructive Examination of PVRC Nozzle Weld Specimen 203 Weld Flaws by JPVRC
By Y. Saiga

(3) Destructive Examination of PVRC Specimen 251J Weld Flaws
By S. Yukawa

The sectioning and examination of Specimens 202 and 203 were sponsored by the Nondestructive Examination Committee of the Japan Pressure Vessel Research Council. The destructive examination of Specimen 251J was performed at the General Electric Company in Schenectady, N.Y., under the sponsorship of the Subcommittee on Nondestructive Examination of Pressure Components of the Pressure Vessel Research Committee of the Welding Research Council. The price of WRC Bulletin 343 is \$24.00 per copy, plus \$5.00 for U.S., or \$8.00 for overseas, postage and handling. Orders should be sent with payment to the Welding Research Council, Room 1301, 345 E. 47th St., New York, NY 10017.

WRC Bulletin 354
June 1990

The two papers contained in this bulletin provide definitive information concerning the elevated temperature rupture behavior of 2¼Cr-1Mo weld metals.

(1) Failure Analysis of a Service-Exposed Hot Reheat Steam Line in a Utility Steam Plant
By C. D. Lundin, K. K. Khan, D. Yang, S. Hilton and W. Zielke

(2) The Influence of Flux Composition of the Elevated Temperature Properties of Cr-Mo Submerged Arc Weldments
By J. F. Henry, F. V. Ellis and C. D. Lundin

The first paper gives a detailed metallurgical failure analysis of cracking in a longitudinally welded hot reheat pipe with 184,000 hours of operation at 1050°F. The second paper defines the role of the welding flux in submerged arc welding of 2¼Cr-1Mo steel.

Publication of this report was sponsored by the Steering and Technical Committees on Piping Systems of the Pressure Vessel Research Council of the Welding Research Council. The price of WRC Bulletin 354 is \$50.00 per copy, plus \$5.00 for U.S. and \$10.00 for overseas postage and handling. Orders should be sent with payment to the Welding Research Council, 345 E. 47th St., Room 1301, New York, NY 10017.